Journal of Superconductivity and Novel Magnetism (2019) 32:911–916
https://doi.org/10.1007/s10948-018-4772-y

ORIGINAL PAPER

Macro- and Nanoscale Magnetic Anisotropy of FeNi(P) Micropillars in Polycarbonate Membrane

S. V. Komogortsev[1] · L. A. Chekanova[1] · E. A. Denisova[1] · A. A. Bukaemskiy[2] · R. S. Iskhakov[1] · S. V. Mel'nikova[1]

Received: 19 April 2018 / Accepted: 7 June 2018 / Published online: 18 June 2018

Abstract

Macroscopic and local magnetic anisotropy of the FeNi(P) pillars deposited using electroless plating in the pores of the nuclear track-etched polycarbonate membrane has been studied. The alloy fills the pores and forms a nail-shaped pillar. The macroscopic easy magnetization axis was found to be perpendicular to the membrane plane due to magnetic shape anisotropy. The macroscopic magnetic anisotropy constant decreases with decreasing pillar diameter from 0.4 to 0.1 μm supposedly due to increase of the pillar cap contribution. Approach to magnetic saturation analysis indicates that the order in local easy magnetization axis is localized on a nanoscale. The correlation length of the local easy axis and the local magnetic anisotropy field in $(Fe_{100-x}Ni_x)_{98}P_2$ pillars of different compositions with diameter of 0.4 μm are studied.

Keywords Magnetic nanowires · Magnetic microwires · Magnetic pillars · Magnetic anisotropy

1 Introduction

Ferromagnetic (FM) nanowires and microwires, pillars or columns are attracting considerable interest due to their unique and tunable magnetic properties and their potential in a wide range of applications: spintronics [1–3], data storage [4], magnetic-field-driven nanowire devices [5], biomagnetism [6–8], bio-sensing [9], microrheology [9], variety of potential medical [8, 10] and therapeutic uses [6, 8]. The shape-induced magnetic anisotropy of magnetic nano- and microwires creates a relatively simple magnetization structure that is being exploited for scientific and technological studies. The high anisotropy of the shape leads to a high uniaxial magnetic anisotropy and associated with it a bistability of magnetic filaments [11–14], as well as the thermal stability of their magnetic properties [15–18]. Morphological defects such as surface roughness, variable diameter, porosity and outgrowths at the ends of filaments due to the features of the particular synthesis technology can greatly influence the magnetic anisotropy [7, 19, 20]. Therefore, a detailed study of the morphology and properties of wires obtained by a particular method is important.

Electrodeposition is the method that can overcome the geometrical restrictions of inserting metals into very deep canals [2, 16, 19, 21–26]. Electroless plating is characterized by much lower deposition rates than electrodeposition [27]. The nucleation can be achieved both at the bottom and on the walls of the pore, thus both the metallic tubes and the wires can be fabricated inside the pores [28–30]. Macroscopic magnetic anisotropy is a natural feature of template-synthesized magnetic materials induced by the shape of the magnetic component and the porosity [19, 22, 31–35]. It restricts the above-mentioned applications. Another important type of anisotropy is the so-called local magnetic anisotropy. It characterizes on-site magnetic anisotropy in amorphous alloys and the magnetic anisotropy of individual crystallite in polycrystalline alloys and it is of interest in concern of tailoring improved soft magnetic properties [35–37]. In this work, both macroscopic and local magnetic anisotropy of the FeNi(P) pillars in polycarbonate membrane are studied.

✉ S. V. Komogortsev
komogor@iph.krasn.ru

[1] Federal Research Center KSC SB RAS, Kirensky Institute of Physics, Krasnoyarsk, 660036, Russia

[2] Institut fur Sicherheitsforschung und Reaktortechnik, 52425 Juelich, Germany

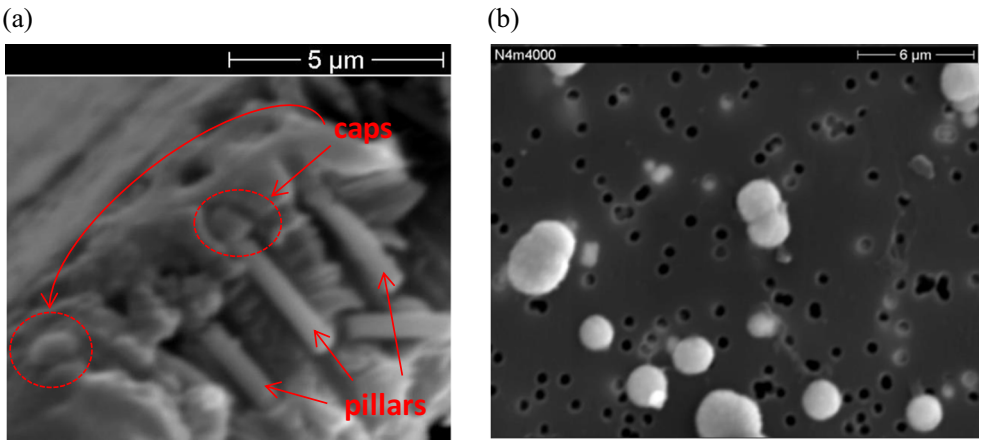

Fig. 1 SEM image of cross section (**a**) and above view (**b**) of the PCTE membrane after electroless plating

2 Experiment

A track-etched 8-μm thick polycarbonate (PCTE) membrane was used as a template for electroless deposition of the $(Fe_{100-x}Ni_x)_{98}(P)_2$ alloy. The monodisperse pores in PCTE membrane are perpendicular to the surface and are distributed randomly over the surface with the mean packing density of 4%. The membranes with different pore diameters from 0.1 up to 0.4 μm were used for electroless deposition. To perform the metal deposition inside PCTE channels, one side of the membrane was coated by a thin layer of thermal-sputtered copper to create an electrochemical potential. Each plating bath was comprised of a source metal ion ($FeSO_4{\cdot}(NH_4)_2SO_4{\cdot}6H_2O$ and $NiCl_2$), a metal chelator, pH stabilizer ($Na_3C_6H_5O_7$, CH_3COONa, buffer solution NH_4Cl), and a reducing agent ($NaPO_2H_2$). The pH of the solution during electroless plating of FeNi(P) columns was kept at 10 and the solution temperature was kept at 80 °C. Deposition was stopped as soon as the metal film on the membrane surface appeared. Afterwards, that film was mechanically removed using tape.

The phosphorus content was determined by the x-ray fluorescence spectrometer (S4 PIONEER, Bruker). Scanning electron microscope SEM-JEOL JSM-840 equipped with energy-dispersive x-ray analysis (EDX) was used for morphologic analysis of the fabricated deposits and exact determination of metal content. X-band ferromagnetic resonance spectra at 9.2 GHz were recorded at room temperatures using a standard EPR spectrometer. The field and temperature dependence of magnetization was measured by a vibrating sample magnetometer.

3 Results and Discussion

Column-shaped metallic inclusions inside the pores aligned perpendicularly to the polycarbonate membrane plane can be seen in the SEM image of cross section of the PCTE membrane with the pore diameter of 0.4 μm after electroless plating (Fig. 1a). The EDX scans that covered the pillars and the caps make it possible to conclude that the pillars and caps are iron-nickel alloy. Quantitatively, the composition was determined by point EDX analysis from the central part of the cap. The hemispheric caps of FeNi(P) columns with diameters in the range from 0.7 to 1.5 μm are revealed at the top surface of the PCTE membrane (Fig. 1b). The composition of pillars FeNi(P) according to EDX analysis is $(Fe_{100-x}Ni_x)_{98}(P)_2$. The detailed composition of the samples (x value) is given in Table 1.

Magnetization curves measured for different orientations (field applied parallel $M^{||}(H)$ and field-applied perpendicular $M^{\perp}(H)$ to the PCTE membrane plane) reveal macroscopic magnetic anisotropy of the fabricated samples (Fig. 2). A quantitative measure of the magnetic anisotropy energy (MAE) is the area enclosed between the $M^{||}(H)$ and $M^{\perp}(H)$ curves [17]. Magnetization curves of three electroless plated PCTE membrane with the same composition of the $(Fe_{85}Ni_{15})_{98}P_2$ alloy but different PCTE membrane pore diameters (0.1, 0.2, and 0.4 μm) show different macroscopic magnetic anisotropy. The maximal MAE with easy magnetization axis perpendicular to PCTE membrane is in the sample with 0.4-μm pore diameter. The sample with 0.2-μm pore diameter is characterized by smaller MAE value but the same easy magnetization axis direction. Finally, the

Table 1 Local magnetic anisotropy field in the $(Fe_{100-x}Ni_x)_{98}P_2$ columns with a diameter of 0.4 μm

x, at.%	5 ± 1	12 ± 2	15 ± 2	26 ± 3	32 ± 3	42 ± 3	54 ± 4
H_a, kOe	1.9	1.6	1.1	1.7	1.0	1.2	1.2
R_c, nm	6 ± 1	6 ± 1	7 ± 2	8 ± 2	8 ± 2	7 ± 2	7 ± 2

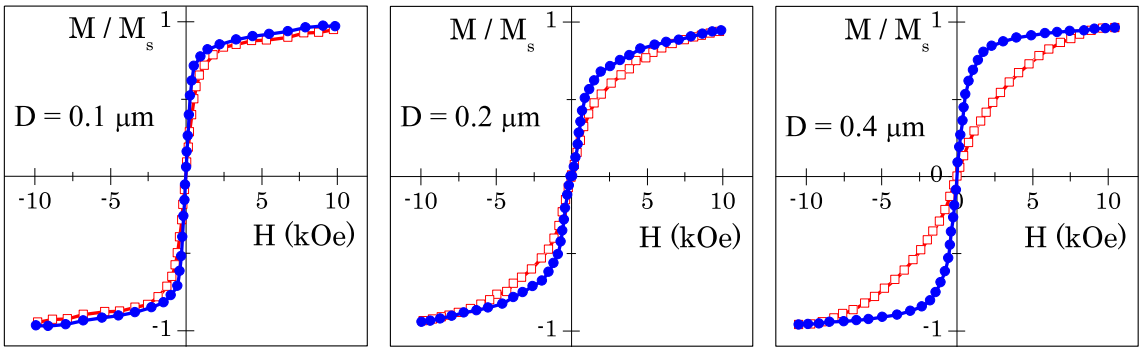

Fig. 2 Magnetization curves in magnetic pillars measured with field applied parallel $M^{||}(H)$ (red empty squares) and with field applied perpendicular $M^{\perp}(H)$ (blue filled circles) to the PCTE membrane plane

sample with 0.1-μm pore diameter is almost magnetically isotropic. This difference is assumed to be due to morphological diversity of the iron-nickel deposit including a pillar and a hemispherical cap. The pillar with high aspect ratio is characterized by easy magnetization axis perpendicular to PCTE membrane plane and the MAE value $E_{\text{la}} = \pi \cdot (M_s)^2$ associated with magnetic shape anisotropy. The hemispherical cap is slightly flattened and should be characterized by easy magnetization plane with certain MAE value E_{ca}. The total MAE value associated with the magnetic shape anisotropy would be the sum $E_{\text{la}} \cdot v - E_{\text{ca}} \cdot (1 - v)$ where v is the volume fraction of the pillars. The value of v is close to the unity for the sample with 0.4-μm pore diameter. But the total MAE value decreases with v as the pore diameter decreases. Actually, dipol-dipol interaction between columns would contribute to the total MAE value as $3P \cdot \pi \cdot (M_s)^2$ where P is the material porosity [38]. In our samples, P is about 0.04 and contribution from magnetic dipol-dipol interaction would be about $0.12 \cdot \pi \cdot (M_s)^2$, i.e. it can be considered negligible in comparison with magnetic shape anisotropy $\pi \cdot (M_s)^2$. Indeed, the magnetic anisotropy field for the sample with 0.4-μm pore diameter is close to magnetic shape anisotropy of elongated column $2\pi \cdot M_s$.

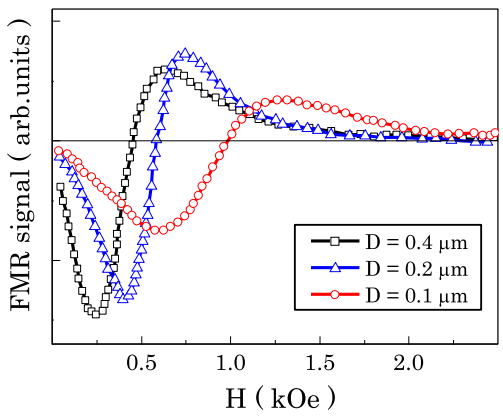

Fig. 3 FMR signal in the pillars with applied field transverse to the PCTE membrane

This explanation is confirmed by FMR data (Fig. 3). Resonance field with the applied field perpendicular to the PCTE membrane plane or along column axis is minimal in the sample with 0.4-μm pore diameter and increases with decreasing pore diameter. This behavior is also due to different shapes of magnetic deposits discussed above [39, 40]. Indeed according to Kittel equation resonance field H_r is [41]:

$$\omega = \gamma \cdot \sqrt{\left[H_r + (N_x - N_z) \cdot M_z\right] \cdot \left[H_r + (N_y - N_z) \cdot M_z\right]} \tag{1}$$

where $\gamma = 1.7 \cdot 10^7$ Hz/Oe, $f = 9.2$ GHz, ($\omega = 2 \cdot \pi \cdot f$), M_z is effective magnetization, and N_x, N_y and N_z are components of demagnetizing factor that directly corresponds to the shape of the ferromagnetic sample (z is along the pillar axis). Since the membrane filled with magnetic pillars is isotropic in the plane, we have $N_x = N_y \neq N_z$. Defining the parameter $\Delta N \equiv N_x - N_z = N_y - N_z$, we obtain an equation for the resonance field of a sample in applied field transverse to the membrane and parallel to the pillars:

$$H_r = \frac{\omega}{\gamma} - \Delta N \cdot M_z \tag{2}$$

We apply (2) only for qualitative consideration since it implies shape of effective ellipsoid instead of the real sample shape. Taking into account that $N_x + N_y + N_z = 4 \cdot \pi$, for a uniform ferromagnetic cylinder elongated along the z-axis ($N_z = 0$), we have $\Delta N = 2 \cdot \pi$. Assuming M_z of the measured samples $(Fe_{85}Ni_{15})_{98}P_2$ to be of about 1500 G [42–44], for a ferromagnetic cylinder, we get a physically meaningless value $H_r < 0$. On the other hand, the shape of pillar's cap is close to the oblate ellipsoid. Thus, for the cap $\Delta N < 0$, i.e. according to (2), $H_r > \frac{\omega}{\gamma} \approx 2.9$ kOe. We observe a single resonance peak in fields of definitely below 2.9 kOe (Fig. 3). This allows us to conclude that the effective value of $\Delta N > 0$. Assuming that elongated cylinder contributes to ΔN as $2 \cdot \pi$ and the contribution of the cap $\Delta N < 0$, we could expect that the effective value

(according to the experiment $\Delta N > 0$), will decrease with increasing the volume fraction of the cap. Assuming that elongated cylinder contributes to ΔN as $2{\cdot}\pi$ and the cap contributes as $\Delta N < 0$, we could expect that the effective value (let us mention that according to the experiment $\Delta N > 0$), will decrease with increase of the volume fraction of the cap. According to (2), this would result to an increase in the resonance field. In view of the above discussion of the effect of the pillar's morphology on the magnetization curves (Fig. 2), this behavior is observed in Fig. 3.

Information on local magnetic anisotropy field one can extract investigating approach magnetization to saturation [37, 45–47]. Next, we discuss approach magnetization to saturation in a series of samples with the same pore diameter (0.4 μm) but different compositions of the FeNi(P) alloy. Such a choice is related to the shape anisotropy of magnetic deposits with the pore diameter 0.4 μm close to elongated cylinder with high aspect ratio. This means that for the $M(H)$ curves measured along pillar axis, the demagnetizing field is negligible and, hence, one can interpret $M(H)$ in terms of internal structure heterogeneity, such as randomly oriented easy magnetization axis of crystallites.

Approach to magnetic saturation plotted in the log-log scale (Fig. 4) according to analyses developed in [32]. Figure 4 reveals $1 - M(H)/M_s \propto H^{-2}$ dependence for H from 6 to 10 kOe and in the field range from 0.5 to 4 kOe, the magnetization approaches saturation as $1 - M(H)/M_s \propto H^{-a}$ with $a \approx 0.65 \pm 0.15$. The crossover in power behavior is observed in the vicinity of the field $H_R = (5.0 \pm 0.1)$ kOe. This is how magnetization is expected to approach saturation in the exchange-coupled system of randomly oriented crystallites [37, 45, 48, 49]. According to theory, the H_R is the exchange field $H_R = 2A/M_s \cdot R_c^2$, where A is the exchange stiffness constant, R_c is the structural correlation length or the average crystallite size $D = R_c$ and M_s is saturation magnetization [45, 50–52]. We fit the piece of $M(H)$ curve where $1 - M(H)/M_s \propto H^{-2}$ by expression $M(H) = M_s\left(1 - \frac{1}{15}(H_a/H)^2\right)$ according to the theory of AMS law, where H_a is the local magnetic anisotropy field or magnetic anisotropy field of one individual crystallite. Obtained values of H_a are listed in the Table 1. Using H_R value ($H_R = 5.0$ kOe), value of exchange stiffness and magnetization value for the Fe–Ni alloys [53], we estimate R_c as $R_c = \sqrt{\frac{2A}{M_s \cdot H_R}}$. According to Table 1, the R_c in different samples are in the range from 6 to 8 nm that implies the order in local easy magnetization axis is localized on a nanoscale and therefore the pillars are nanocrystalline [37].

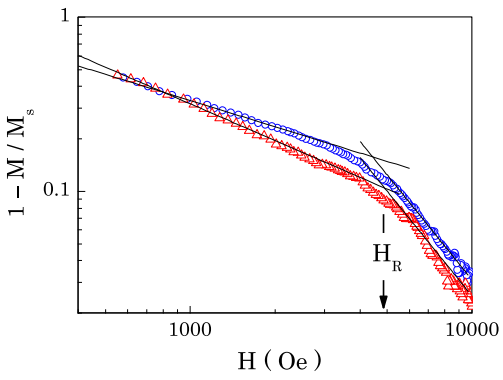

Fig. 4 Approach magnetization to saturation in the pillars with a pore diameter of 0.4 μm (double logarithmic scale). Red triangles correspond to $(Fe_{88}Ni_{12})_{98}P_2$ pillars, blue circles correspond to $(Fe_{74}Ni_{26})_{98}P_2$ pillars. Solid lines visualize power dependences below and above H_R

The values of grain size only slightly vary with alloy composition but crystallite anisotropy is very sensitive to alloy composition. The effective constant of local magnetic anisotropy of iron-nickel alloys includes magneto-crystalline anisotropy, anisotropy induced by internal stresses in crystallite, shape anisotropy and surface anisotropy. In nanocrystalline alloys, these contributions can turn out to be comparable to each other [54]. Here, we cannot separate these contributions but still give a qualitative discussion of the data within at least one of the contributions. The H_a is minimal at two concentrations 15 and 32 at.% Ni (Table 1). The concentration of 32 at.% Ni is associated with the formation of Invar alloy, the magnetization in which is sharply reduced, which in turn leads to a decrease in the magnetic anisotropy constant. This feature is observed experimentally [55]. In the bcc Fe–Ni alloys with the Ni content up to 18 at.% the anisotropy constant decreases with increasing nickel concentration [56]. The increased H_a at $x = 26\%$ may be due to the growth of internal stresses near the invar composition, due to the formation of a two-phase structure of bcc + fcc.

4 Conclusions

The macroscopic and local magnetic anisotropy of the FeNi(P) pillars electroless deposited in the pores of the nuclear track etched polycarbonate membrane has been studied. The morphological diversity of iron-nickel deposit includes pillars and hemispherical caps. The macroscopic magnetic anisotropy is maximal for the pillars with a diameter of 0.4 μm and its easy magnetization axis is along the pillar axis and therefore is perpendicular to the membrane surface. The energy of macroscopic magnetic anisotropy decreases with decreasing pore diameter and almost disappears in pillars with a diameter of 0.1 μm. Approach to magnetic saturation indicates that the investigated FeNi(P)

pillars are nanocrystalline. The local magnetic anisotropy energy and the correlation radii (about 7 nm) of the local magnetic anisotropy in nanocrystalline Fe–Ni(P) microcolumns are determined. These radii only slightly vary with alloy composition but the crystallite anisotropy field is very sensitive to alloy composition.

References

1. Piraux, L., Dubois, S., Duvail, J., Ounadjela, K., Fert, A.: Arrays of nanowires of magnetic metals and multilayers: perpendicular GMR and magnetic properties. J. Magn. Magn. Mater. **175**, 127–136 (1997)
2. Fert, A., Piraux, L.: Magnetic nanowires. J. Magn. Magn. Mater. **200**, 338–358 (1999). https://doi.org/10.1016/S0304-8853(99)00375-3
3. Darques, M., Spiegel, J., De la Torre Medina, J., Huynen, I., Piraux, L.: Ferromagnetic nanowire-loaded membranes for microwave electronics. J. Magn. Magn. Mater. **321**, 2055–2065 (2009). https://doi.org/10.1016/j.jmmm.2008.03.060
4. Irshad, M.I., Ahmad, F., Mohamed, N.M.: A review on nanowires as an alternative high density magnetic storage media. Presented at the (2012)
5. Vázquez, M.: Advanced magnetic microwires. In: Handbook of Magnetism and Advanced Magnetic Materials. Wiley, Chichester (2007)
6. Safi, M., Yan, M., Guedeau-Boudeville, M.-A., Conjeaud, H., Garnier-Thibaud, V., Boggetto, N., Baeza-Squiban, A., Niedergang, F., Averbeck, D., Berret, J.-F.: Interactions between magnetic nanowires and living cells: uptake, toxicity, and degradation. ACS Nano. **5**, 5354–5364 (2011). https://doi.org/10.1021/nn201121e
7. Fratila, R.M., Rivera-Fernández, S., de la Fuente, J.M.: Shape matters: synthesis and biomedical applications of high aspect ratio magnetic nanomaterials. Nanoscale **7**, 8233–8260 (2015). https://doi.org/10.1039/C5NR01100K
8. Reich, D.H., Tanase, M., Hultgren, A., Bauer, L.A., Chen, C.S., Meyer, G.J.: Biological applications of multifunctional magnetic nanowires (invited). J. Appl. Phys. **93**, 7275–7280 (2003). https://doi.org/10.1063/1.1558672
9. Alfadhel, A., Li, B., Zaher, A., Yassine, O., Kosel, J.: A magnetic nanocomposite for biomimetic flow sensing. Lab Chip **14**, 4362–4369 (2014). https://doi.org/10.1039/C4LC00821A
10. Ivanov, Y.P., Alfadhel, A., Alnassar, M., Perez, J.E., Vazquez, M., Chuvilin, A., Kosel, J.: Tunable magnetic nanowires for biomedical and harsh environment applications. Sci. Rep. **6**, 24189 (2016). https://doi.org/10.1038/srep24189
11. Varga, R., Klein, P., Sabol, R., Richter, K., Hudak, R., Polaček, I., Praslicka, D., Šmelko, M., Hudak, J., Mikita, I., Badini-Confalonieri, G.A., El Kammouni, R., Vazquez, M.: Magnetically bistable microwires: properties and applications for magnetic field, temperature, and stress sensing. Presented at the (2017)
12. Zhukov, A., Ipatov, M., Zhukova, V.: Processing magnetic microwires for magnetic bistability and magnetoimpedance. In: Magnetic Nano- and Microwires, pp. 225–274. Elsevier (2015)
13. Rodionova, V., Chichay, K., Zhukova, V., Perov, N., Ipatov, M., Umnov, P., Molokanov, V., Zhukov, A.: Tailoring of magnetic properties of amorphous ferromagnetic microwires. J. Supercond. Nov. Magn. **28**, 977–981 (2015). https://doi.org/10.1007/s10948-014-2777-8
14. Zhukov, A., Talaat, A., Ipatov, M., del Val, J.J., Gonzalez-Legarreta, L., Hernando, B., Chizhik, A., Blanco, J.M., Zhukova, V.: Optimization of magnetic properties and giant magnetoimpedance effect in nanocrystalline microwires. J. Supercond. Nov. Magn. **28**, 813–822 (2015). https://doi.org/10.1007/s10948-014-2654-5
15. Shumskaya, A.E., Kaniukov, E.Y., Kozlovskiy, A.L., Zdorovets, M.V., Rusakov, V.S., Kadyrzhanov, K.K.: Structure and physical properties of iron nanotubes obtained by template synthesis. Phys. Solid State **59**, 784–790 (2017). https://doi.org/10.1134/S1063783417040266
16. Zagorskiy, D.L., Artemov, V.V., Korotkov, V.V., Kruglikov, S.S., Bedin, S.A.: Specific features of the growth and stability of nanowires made of different metals. J. Surf. Invest.: X-ray, Synchrotron Neutron Tech. **11**, 99–106 (2017). https://doi.org/10.1134/S1027451016050633
17. Komogortsev, S.V., Iskhakov, R.S., Denisova, E.A., Balaev, A.D., Myagkov, V.G., Bulina, N.V., Kudashov, A.G., Okotrub, A.V.: Magnetic anisotropy in the films of oriented carbon nanotubes filled with iron nanoparticles. Tech. Phys. Lett. **31**, 454–456 (2005). https://doi.org/10.1134/1.1969761
18. Ahmad, N., Chen, J.Y., Zhou, W.P., Liu, D.P., Han, X.F.: Magnetoelastic anisotropy induced effects on field and temperature dependent magnetization reversal of Ni nanowires and nanotubes. J. Supercond. Nov. Magn. **24**, 785–792 (2011). https://doi.org/10.1007/s10948-010-1016-1
19. Nasirpouri, F., Peighambari, S.M., Samardak, A.S., Ognev, A.V., Sukovatitsina, E.V., Modin, E.B., Chebotkevich, L.A., Komogortsev, S.V., Bending, S.J.: Electrodeposited Co93.2P6.8 nanowire arrays with core-shell microstructure and perpendicular magnetic anisotropy. J. Appl. Phys. **117**, 17E715 (2015). https://doi.org/10.1063/1.4919124
20. Nasirpouri, F., Sanaeian, M.R., Samardak, A.S., Sukovatitsina, E.V., Ognev, A.V., Chebotkevich, L.A., Hosseini, M.-G., Abdolmaleki, M.: An investigation on the effect of surface morphology and crystalline texture on corrosion behavior, structural and magnetic properties of electrodeposited nanocrystalline nickel films. Appl. Surf. Sci. **292**, 795–805 (2014). https://doi.org/10.1016/j.apsusc.2013.12.053
21. Bantu, A.K.M., Rivas, J., Zaragoza, G., López-Quintela, M.A., Blanco, M.C.: Structure and magnetic properties of electrodeposited cobalt nanowires. J. Appl. Phys. **89**, 3393 (2001). https://doi.org/10.1063/1.1345857
22. Chiriac, H., Moga, A.-E., Urse, M., Paduraru, I., Lupu, N.: Preparation and magnetic properties of amorphous NiP and CoP nanowire arrays. J. Magn. Magn. Mater. **272–276**, 1678–1680 (2004). https://doi.org/10.1016/j.jmmm.2003.12.540
23. Nasirpouri, F.: Template electrodeposition of nanowires arrays. Presented at the (2017)
24. Frolov, K.V., Zagorskii, D.L., Lyubutin, I.S., Chuev, M.A., Perunov, I.V., Bedin, S.A., Lomov, A.A., Artemov, V.V., Sulyanov, S.N.: Magnetic and structural properties of Fe–Co nanowires fabricated by matrix synthesis in the pores of track membranes. JETP Lett. **105**, 319–326 (2017). https://doi.org/10.1134/S0021364017050083
25. Najafi, M., Alemipour, Z., Hasanzadeh, I., Aftabi, A., Soltanian, S.: Influence of annealing temperature, electrolyte concentration and electrodeposition conditions on magnetic properties of electrodeposited Co-Cr alloy nanowires. J. Supercond. Nov. Magn. **28**, 95–101 (2015). https://doi.org/10.1007/s10948-014-2803-x
26. Mehri, A., Seyyed Ebrahimi, S.A., Abdizadeh, H.: Optimization of the sol–gel chemical route for fabrication of densely packed NiFe2O4 nanowires in the AAO template. J. Supercond. Nov. Magn. **25**, 2047–2052 (2012). https://doi.org/10.1007/s10948-012-1561-x

27. Sudagar, J., Lian, J., Sha, W.: Electroless nickel, alloy, composite and nano coatings—a critical review. J. Alloys Compd. **571**, 183–204 (2013). https://doi.org/10.1016/j.jallcom.2013.03.107
28. Wang, W., Li, N., Li, X., Geng, W., Qiu, S.: Synthesis of metallic nanotube arrays in porous anodic aluminum oxide template through electroless deposition. Mater. Res. Bull. **41**, 1417–1423 (2006)
29. Zhang, Z., Dai, S., Blom, D., Shen, J.: Synthesis of ordered metallic nanowires inside ordered mesoporous materials through electroless deposition. Chem. Mater. **14**, 965–968 (2002)
30. Rohan, J.F., Casey, D.P., Ahern, B.M., Rhen, F.M.F., Roy, S., Fleming, D., Lawrence, S.E.: Coaxial metal and magnetic alloy nanotubes in polycarbonate templates by electroless deposition. Electrochem. Commun. **10**, 1419–1422 (2008). https://doi.org/10.1016/j.elecom.2008.07.019
31. Aravamudhan, S., Singleton, J., Goddard, P.A., Bhansali, S.: Magnetic properties of Ni–Fe nanowire arrays: effect of template material and deposition conditions. J. Phys. D. Appl. Phys. **42**, 115008 (2009). https://doi.org/10.1088/0022-3727/42/11/115008
32. Henry, Y., Ounadjela, K., Piraux, L., Dubois, S., George, J.-M., Duvail, J.-L.: Magnetic anisotropy and domain patterns in electrodeposited cobalt nanowires. Eur. Phys. J. B **20**, 35–54 (2001). https://doi.org/10.1007/s100510170283
33. Ebels, U., Duvail, J., Wigen, P., Piraux, L., Buda, L., Ounadjela, K.: Ferromagnetic resonance studies of Ni nanowire arrays. Phys. Rev. B **64**, 144421 (2001). https://doi.org/10.1103/PhysRevB.64.144421
34. Samardak, A.S., Nasirpouri, F., Nadi, M., Sukovatitsina, E.V., Ognev, A.V., Chebotkevich, L.A., Komogortsev, S.V.: Conversion of magnetic anisotropy in electrodeposited Co–Ni alloy nanowires. J. Magn. Magn. Mater. **383**, 94–99 (2015). https://doi.org/10.1016/j.jmmm.2014.10.047
35. Samardak, A.S., Ognev, A.V., Samardak, A.Y., Stebliy, E.V., Modin, E.B., Chebotkevich, L.A., Komogortsev, S.V., Stancu, A., Panahi-Danaei, E., Fardi-Ilkhichy, A., Nasirpouri, F.: Variation of magnetic anisotropy and temperature-dependent FORC probing of compositionally tuned Co-Ni alloy nanowires. J. Alloys Compd. **732**, 683–693 (2018). https://doi.org/10.1016/j.jallcom.2017.10.258
36. Herzer, G.: Modern soft magnets: amorphous and nanocrystalline materials. Acta Mater. **61**, 718–734 (2013). https://doi.org/10.1016/j.actamat.2012.10.040
37. Iskhakov, R.S., Komogortsev, S.V.: Magnetic microstructure of amorphous, nanocrystalline, and nanophase ferromagnets. Phys. Met. Metallogr. **112**, 666–681 (2011). https://doi.org/10.1134/S0031918X11070064
38. Encinas-Oropesa, A., Demand, M., Piraux, L., Huynen, I., Ebels, U.: Dipolar interactions in arrays of nickel nanowires studied by ferromagnetic resonance. Phys. Rev. B **63**, 104415 (2001). https://doi.org/10.1103/PhysRevB.63.104415
39. Ebels, U., Duvail, J.-L., Wigen, P.E., Piraux, L., Buda, L.D., Ounadjela, K.: Ferromagnetic resonance studies of Ni nanowire arrays. Phys. Rev. B **64**, 144421 (2001). https://doi.org/10.1103/PhysRevB.64.144421
40. Iskhakov, R.S., Komogortsev, S.V., Chekanova, L.A., Balaev, A.D., Yuzova, V.A., Semenova, O.V.: The magnetic structure of ferromagnetic filaments of a CoNi(P) alloy in a porous silicon matrix. Tech. Phys. Lett. **29**, 263–266 (2003). https://doi.org/10.1.1573285
41. Kittel, C.: On the theory of ferromagnetic resonance absorption. Phys. Rev. **73**, 155–161 (1948). https://doi.org/10.1103/PhysRev.73.155
42. Rusov, G.I.: Ferromagnetic and spin-wave resonance in thin Fi-Ni films. Sov. Phys.-Solid State **9**, 146 (1967)
43. Adachi, K., Bonnenberg, D., Hempel, K.A., Wijn, H.P.J.: Alloys between 3d elements. In: Magnetic Properties of Metals, p. 142 (1986)
44. Bozorth, R.M.: Ferromagnetism. Van Nostrand, Princeton (1968)
45. Chudnovsky, E.M., Saslow, W.M., Serota, R.A.: Ordering in ferromagnets with random anisotropy. Phys. Rev. B **33**, 251–261 (1986)
46. Samardak, A.S., Ognev, A.V., Samardak, A.Y., Stebliy, E.V., Modin, E.B., Chebotkevich, L.A., Komogortsev, S.V., Stancu, A., Panahi-Danaei, E., Fardi-Ilkhichy, A., Nasirpouri, F.: Variation of magnetic anisotropy and temperature-dependent FORC probing of compositionally tuned Co-Ni alloy nanowires. J. Alloys Compd. **732**, 683–693 (2018). https://doi.org/10.1016/j.jallcom.2017.10.258
47. Komogortsev, S.V., Iskhakov, R.S.: Law of approach to magnetic saturation in nanocrystalline and amorphous ferromagnets with improved transition behavior between power-law regimes. J. Magn. Magn. Mater. **440**, 213–216 (2017). https://doi.org/10.1016/j.jmmm.2016.12.145
48. Iskhakov, R.S., Ignatchenko, V.A., Komogortsev, S.V., Balaev, A.D.: Study of magnetic correlations in nanostructured ferromagnets by correlation magnetometry. J. Exp. Theor. Phys. Lett. **78**, 646–650 (2003). https://doi.org/10.1134/1.1644310
49. Iskhakov, R.S., Komogortsev, S.V., Balaev, A.D., Chekanova, L.A.: Dimensionality of a system of exchange-coupled grains and magnetic properties of nanocrystalline and amorphous ferromagnets. J. Exp. Theor. Phys. Lett. **72**, 304–307 (2000). https://doi.org/10.1134/1.1328443
50. Thomas, L., Tuaillon, J., Perez, J.P., Dupuis, V., Perez, A., Barbara, B.: Approach to saturation in nanocrystallized films of iron and nickel. J. Magn. Magn. Mater. **140–144**, 437–438 (1995). https://doi.org/10.1016/0304-8853(94)00728-4
51. Perez, J., Dupuis, V., Tuaillon, J., Perez, A., Paillard, V., Mellinon, P., Treilleux, M., Thomas, L., Barbara, B., Bouchet-Fabre, B.: Magnetic properties of nanostructured iron films obtained by low energy neutral cluster beam deposition. J. Magn. Magn. Mater. **145**, 74–80 (1995)
52. Dupuis, V., Perez, J.P., Tuaillon, J., Paillard, V., Mélinon, P., Perez, A., Barbara, B., Thomas, L., Fayeulle, S., Gay, J.M.: Magnetic properties of nanostructured thin films of transition metal obtained by low energy cluster beam deposition. J. Appl. Phys. **76**, 6676 (1994). https://doi.org/10.1063/1.358165
53. Coey, J.M.D.: Magnetism and Magnetic Materials. Cambridge University Press, New York (2010)
54. Harin, E.V., Sheftel, E.N.: Micromagnetic structure of soft magnetic nanocrystalline Fe-based films. Phys. Met. Metallogr. **116**, 753–759 (2015). https://doi.org/10.1134/S0031918X15080074
55. Vazhenina, I.G., Iskhakov, R.S., Chekanova, L.A.: Spin-wave resonance in chemically deposited Fe-Ni films: measuring the spin-wave stiffness and surface anisotropy constant. Phys. Solid State **60**, 292–298 (2018). https://doi.org/10.1134/S1063783418020294
56. Tarasov, L.P.: Ferromagnetic anisotropy of low nickel alloys of iron. Phys. Rev. **56**, 1245–1246 (1939). https://doi.org/10.1103/PhysRev.56.1245.2